ChemistrySelect

Research Article
doi.org/10.1002/slct.202304825

Chemistry Europe
European Chemical Societies Publishing

www.chemistryselect.org

Hydrothermal Synthesis of Tartaric Acid Functionalized Amino Acid CQD for Sensing of Hg^{2+} and Fe^{3+} Ions in Aqueous Medium

Geeta A. Zalmi,*[a] Pritesh Khobrekar,[b] Ratan W. Jadhav,[b] Ronita R. Naik,[a] Shreya Sinari,[a] Sandesh T. Bugde,[b] and Sheshanath V. Bhosale*[c]

Carbon quantum dots (CQDs) are a type of carbon-based nanoparticles that are typically smaller than 10 nanometres in size. In this study, L-tryptophan-mediated CQDs were synthesized using the hydrothermal carbonization (HTC) technique, which is known for its non-toxic, environmentally friendly, and cost-effective nature. The synthesized carbon quntum dot was successfully characterized. The HR-TEM analysis clearly revealed the formation of specific aggregates with a size distribution ranging from 3.0 to 5.1 nm. These L-tryptophan-mediated CQDs exhibited remarkable emission behaviour, displaying strong and stable blue fluorescence. Moreover, they were utilized as a sensor for the sensitive detection of Fe^{3+} and Hg^{2+} ions in an aqueous solution, employing a fluorescence quenching mechanism. The limit of detection for Fe^{3+} sensing was determined to be 1.2×10^{-5} M, while for Hg^{2+} sensing, it was found to be 1.9×10^{-5} M. The sensing of Fe^{3+} and Hg^{2+} ions was also confirmed through visual eye detection, as a significant color change of the CQDs was observed. Additionally, a competitive study was conducted to verify the selectivity of the L-tryptophan-mediated CQDs towards Fe^{3+} and Hg^{2+} metal ions.

1. Introduction

Carbon, also known as black material, is one of the most abundant elements in nature.[1] In recent years, low-dimensional carbon-based nanoparticles such as fullerene, carbon dots, carbon nanotubes, and graphene have received great research attention due to their easy availability and functionalization.[2] Nevertheless, except for carbon dots, other carbon-based materials have been shown to have very low solubility in water and weak fluorescence. To overcome these issues, researchers have focused on the development of functionalized carbon dots (CQDs) for various applications, as CQDs are shown to be highly soluble in water and produce strong luminescence.[3] These zero-dimensional carbon dots have become increasingly popular due to not only their antimicrobial activities but also their antioxidant properties in food preservation.[4] Regardless of the difference in their core structure, carbon dots can easily be functionalized using a variety of functional groups, including amino, epoxy, hydroxy, and carboxy groups.[4–6] CQDs are resistant to photobleaching and offer tunable physicochemical and optical properties. Importantly, CQDs have shown to be relatively low toxic, which provides alternatives to fluorescent dyes and heavy metal-based quantum dots.[7–9]

Many different approaches have been presented to synthesize CQDs. Mainly, two routes have been widely used: the first one is top-down, and the second one is bottom-up methods. The top-down method in which CQDs are synthesized from larger carbon materials[10]. In contrast, in the bottom-up procedure, the CQDs are acquired from molecular precursors.[11] CQDs are synthesized in numerous ways, such as by laser ablation, pyrolysis, arc discharge, and nitric acid/sulfuric oxidation methods. These methods showed downsides such as complex synthesis techniques, harsh climate, low quantum yields, high cost, and environmental destruction.[12] In 2004, Xu *et al.* unintentionally discovered carbon nanoparticles with fluorescent properties when they first separated single-walled carbon nanotubes employing gel electrophoresis from carbon soot produced by arc discharge.[13] Later, Sun *et al.* developed the synthesis of CQDs of graphite powder using a carrier gas such as argon in the presence of water vapor by laser ablation and successfully utilizing them in multi-photon imaging.[14] In recent years, fluorescence (FL) based sensing has gained much attention due to its benefits, such as magnificent sensitivity, low cost, and short response time. Carbon dot size and surface chemical groups can be carefully regulated to acquire fluorescent properties.[15]

Due to their abundant surface groups, fluorescent CQD possesses a strong ability to bind with other organic and inorganic molecules. Thus, fluorescent CQD can be manipulated *via* a series of controllable chemical treatments.[13] Fluorescent nanomaterials have further amplified the interest of researchers by the fact that they can be synthesized from relatively inexpensive sources, including simple organic molecules such as citric acid or more heterogeneous sources that include

[a] G. A. Zalmi, R. R. Naik, S. Sinari
DCT's Dhempe College of Arts and Science, Miramar, Panjim, Goa-403001
E-mail: geetazalmi446@gmail.com

[b] P. Khobrekar, R. W. Jadhav, S. T. Bugde
School of Chemical Sciences, Goa University, Talieigao, Goa 403206 India

[c] Prof. S. V. Bhosale
Department of Chemistry, School of Chemical Sciences, Central University of Karnataka, Kalaburgi-585367, Karnataka, India
E-mail: bsheshanath@cuk.ac.in

Supporting information for this article is available on the WWW under https://doi.org/10.1002/slct.202304825

orange juice, rice, coffee beans, ashes, neem leaves, mango peel, rose petals or even waste.[16] The factors that influence the fluorescence of CQDs are the pH, solvent, and metal ion effects. CQDs have been reported for several applications ranging from photoelectrical conversion, light-emitting devices, photocatalysis, bioimaging, sensing, drug delivery, metal ion probe, and theranostic to enzyme activity.[17] CQDs can also be useful in biosensing as biosensor applications.

Various supramolecular sensors have been announced for the selective and sensitive detection of cations, anions, and neutral species.[8] Currently, there is an increasing demand for quantification and highly selective detection of metal ions for a variety of industrial, environmental, biological, and health applications. Unstable ferrous (Fe^{2+}) ions and stable ferric (Fe^{3+}) ions are of special significance; Fe^{2+} under aerobic aqueous environments tends to oxidize to the Fe^{3+} form. Therefore, a fast and accurate determination of iron ions is a serious issue in both the biological system and the environment.[18,19] The heavy metal ion Hg(II) causes many diseases and poses a serious threat to the ecological community and common health due to the rapid growth of the industry, which produces large amounts of Hg(II) waste. Therefore, there is a need to develop simple techniques that are of great significance to detect Hg(II) for environmental guarding and human health monitoring.[20]

In this work, we describe the synthesis of promising fluorescent carbon dots by a one-step hydrothermal method. CQDs were functionalized with an amino acid, which is the building block of proteins and peptides, which consists of chemical and physical properties with the presence of positive and negative charges with a hydrophobic nature along with the aromatic functional group.[21,22,23] These functional moieties play a key role in molecular interactions.[24] In particular, we have prepared CQDs by hydrothermal methods using L-tryptophan and tartaric acid (coded as CQD-TA-TRYP). After synthesis, the amino acid functionalized CQD was systemically characterized by FTIR-spectroscopy and their photophysical properties were studied by UV-Vis and fluorescence spectrometry. Furthermore, CQD-TA-TRYP was effectively utilized for the selective detection of Hg^{2+} and Fe^{3+} ions over other biologically competitive ions.

2. Results and Discussion

2.1. Characterization of CQD-TA-TRYP

Furthermore, the CQD-TA-TRYP was characterized by HR-TEM to investigate their particle size distribution to study the surface morphology and shape of the CQD-TA-TRYP. HR-TEM clearly shows the formation of monodispersed nanoparticles with spherical shapes. Figure 1a and 1b shows the HR-TEM micrograph and particle size distribution plot, respectively. It was observed that the CQD-TA-TRYP were well distributed in the range of 3.0 nm to 5.2 nm size. The synthesized CQDs were characterized by infrared spectroscopy (IR) to investigate the presence of functional groups on the surface of the CQD-TA-TRYP Figure S3. As can be seen, the presence of N–H and COOH functional groups appears at 3162 cm^{-1}. While carbonyl stretching frequency was observed at 1683 cm^{-1}, 1055 cm^{-1} corresponds to the C–O functional group, 1582 cm^{-1} corresponds to $-COO^-$, whereas 1393 cm^{-1} corresponds to the -CONH functional group, respectively. These indicate the CQD-TA-Tryp is highly surface functionalized with COOH, NH, and –OH groups.

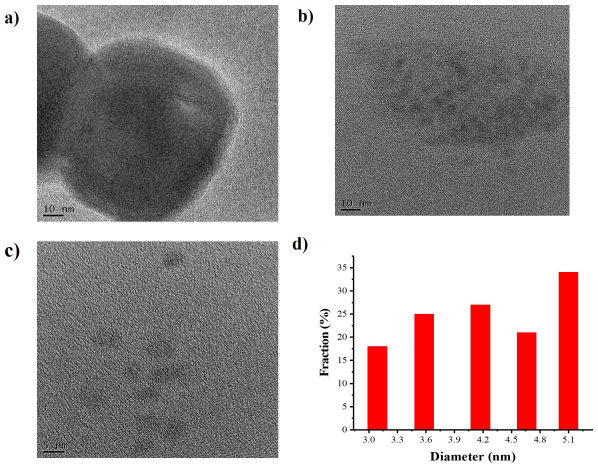

Figure 1. (a, b) HR-TEM image (10 nm), (c) HR-TEM image, (5 nm) d) Diameter distribution plot.

2.2. X-Ray Powder Diffraction (XRD)

XRD pattern was recorded using powder XRD – Rigaku Smartlab X-ray diffractometer with X-ray source CuKα radiation. The sample was placed on silicon low background sample holder which was subjected to theta to 2θ scan. It was observed that the synthesized carbon dot showed intense peak of crabon at 27.14 θ this confirms that the CQD-TA-TRYP was successfully synthesized. Figure 2.

2.3. Optical Properties

The synthesized CQD-TA-TRYP was examined for their absorption and fluorescent properties, as shown in Figure 2. In the

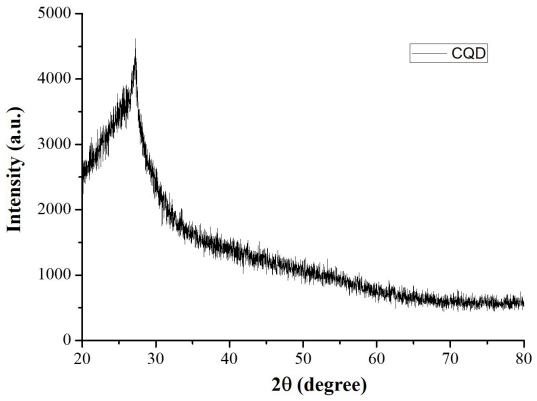

Figure 2. Powder XRD Pattern for the synthesized CQD-TA-TRYP.

absorption study, it is revealed that CQD-TA-TRYP shows an intense absorption band at 231 nm that corresponds to the π–π transition of C=C bonds and C=N groups. While a small broad absorption band appears near 250 nm to 300 nm, attributing to n–π* transition due to the carbonyl group. Further, the absorption after 300 nm tails throughout the 40 nm is due to low transition functional groups attached to the sp^2 hybridized carbon dot. Furthermore, upon excitation at wavelength 320 nm, CQDs produce a bright blue fluorescent color with an emission band at 400 nm.

After the optical properties and fluorescence properties of the synthesized carbon dot were recorded by subjecting it to various solvent systems, the emission spectra were recorded in different solvents such as dimethyl sulphoxide (DMSO), tetrahydrofuran (THF), acetonitrile (MeCN), dimethylformamide (DMF), and Distilled Water (DW). The fluorescent carbon dot shows fluorescence at 400 nm for all the organic solvents and distilled water. However, the highest fluorescence intensity was observed only in distilled water. While it is observed from Figure 3. that the carbon dot showed high fluorescence in distilled water compared to another solvent, this indicates the synthesized carbon dot shows excellent fluorescence properties compared with other solvents. Therefore, for further analysis, the carbon dots studied were performed using distilled water as a suitable solvent for analysis. The differences in the fluorescence emission property were mainly due to the solvatochromic effect observed for the ground state and excited state for CQD-TA-TRYP in various organic solvents.

The excitation-dependent study was performed for the CQD-TA-TRYP with the increasing wavelength from 250 nm to 460 nm, as shown in Figure 4a. The red shift was observed for the CQD-TA-TRYP in distilled water this is because of the presence of functional groups on the CQD surface with different energy states upon excitation at different wavelengths. Therefore, the CQD shows emissions in different energy states. Sometimes, not only the functional group at CQD's surface show the fluorescence, but particle size and its distribution also play a very important role in studying the energy states of CQD. The fluorescence quantum yield was calculated by using quinine sulfate as the reference for the CQD-TA-TRYP, and it was observed that the CQD-TA-TRYP was 7.6% shown in Figure 4a. in distilled water.

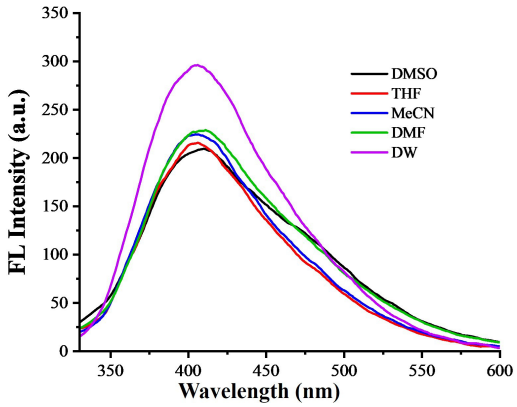

Figure 3. Fluorescence emission spectra of CQD-TA-TRYP in various solvents (λ_{ex} = 320 nm).

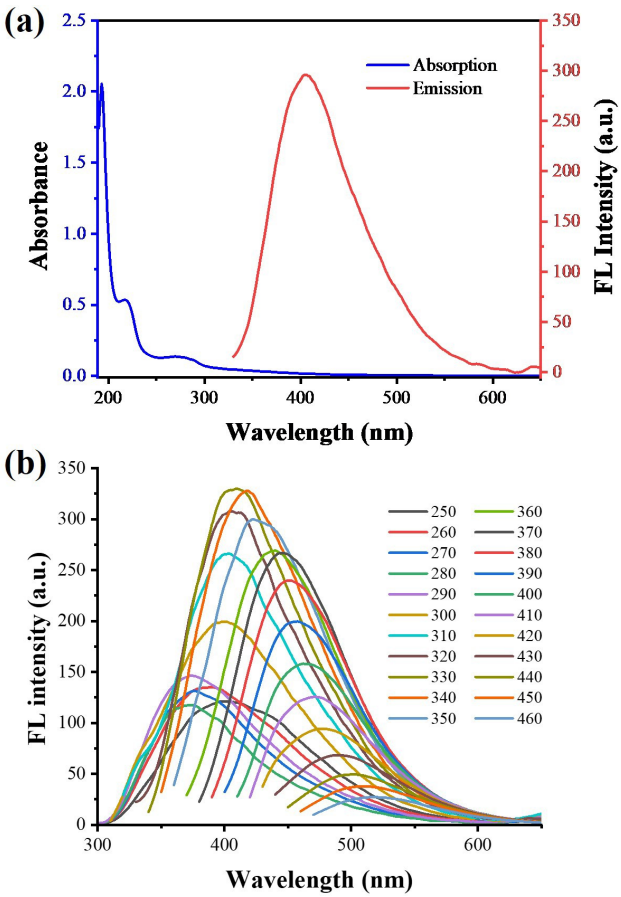

Figure 4. a) UV-vis absorption and emission spectra in DW (excitation wavelength = 320 nm), (b) Fluorescence emission spectra of CQD-TA-TRYP in DW at diverse excitation wavelengths.

3. Effect of PH

pH is an important physiological parameter that needs to be considered in various biological processes in every field. Thus, the synthesized carbo dot was examined for the effect of pH on its photophysical properties. From the pH study, it was revealed that the CQD-TA-TRYP showed a decrease in fluorescence at pH 4, while at pH 9 and pH 7, there was no change observed in fluorescence. This change may be due to the protonation or deprotonation taking place at the surface of the synthesized carbon dot. The pH study indicated that the carbon dot was relatively less stable at pH 4. As shown in Figure S1.

4. Fluorimetric Detection

To study its selectivity towards various metal ions, fluorometric sensing has proven to be an excellent tool. Its effective fluorescence properties make the CQD-TA-TRYP a very important chemosensor for sensing metal ions and various biomole-

cules. The fluorescence sensing property is examined by the turn-off and turn-on behaviour of CQD when it shows binding toward a particular analyte. In this study, the synthesized CQD-TA-TRYP showed excellent colorimetric and fluorescence properties and were found to be highly selective towards Fe^{3+} and Hg^{2+} ions. Furthermore, its photophysical changes with the addition of Fe^{3+} and Hg^{2+} were investigated by fluorescence experiments.

5. Naked Eye

The naked eye detection study was performed by preparing the stock solution of the CQD-TA-TRYP. All the experiments were performed in distilled water. First, the stock solution of CQD was prepared in distilled water (1 ml of CQD-TA-TRYP in 10 ml DW), followed by the preparation of metal ion analyte solution in DW (1 mM). Metal ions such as $FeCl_3$, $CuCl_2$, $CaCl_2$, $NiCl_2$, $CoCl_2$, $Zn(NO_3)_2$, $CdCl_2$, $PbSO_4$, $Al(NO_3)_3$, $HgCl_2$, $BaSO_4$, $MnCl_2$, and $SnCl_2$. The sensing study was performed by adding various metal ions to the stock solution of CQD. After the addition of all metal ions, the solution was kept under 365 nm. It was observed that the solution of CQD showed quenching of fluorescence with the addition of Fe^{3+} and Hg^{2+} metal ions, while other metal ions did not show any change in fluorescence. Figure 5. The sensing properties of the CQD-TA-TRYP were further confirmed by performing UV-Vis absorption and fluorescence emission spectroscopy. In addition, its competitive study was performed to confirm its selectivity towards Fe^{3+} and Hg^{2+} metal ions.

6. UV-Vis and Fluorescence Response of CQD-TA-TRYP to Fe^{3+} and Hg^{2+} Ions

The selectivity towards various cations and their interaction was investigated by performing a UV-Vis Spectroscopic study. The absorption and emission spectra were recorded for CQD in the presence and absence of Fe^{3+} and Hg^{2+} ions. The CQD showed an absorption maximum at 230 nm and a broad peak at 300 nm region. However, the emission spectra for the CQD-TA-TRYP were observed at 400 nm, as shown in Figure 7.

The fluorescence spectroscopic study was performed for CQD-TA-TRYP with the addition of various cations, as shown in the figure. In this study, the Tryp-CQD were excited at 320 nm, and different cations were added, such as Pb^{2+}, Fe^{3+}, Hg^{2+}, Al^{3+}, Co^{2+}, Cu^{2+}, Ni^{2+}, Zn^{2+}, Cd^{2+}, Mn^{2+}, Ba^{2+}, Fe^{2+}, and Sn^{3+} to the solutions containing CQD. It is observed from the plot that the CQD was highly selective towards Hg^{2+} and Fe^{3+} metal ions in the presence of other cations, with an abrupt decrease in fluorescence intensity with Fe^{3+} and Hg^{2+} at 400 nm. The CQD presenting blue fluorescence completely disappeared or quenched completely in the presence of Hg^{2+} and Fe^{3+} metal ions however, no change in fluorescence intensity was observed for other metal ions. The change in absorption spectra was observed with addition of Hg^{2+} and Fe^{2+} metal ion. The following change was observed as shown in Figure 6.

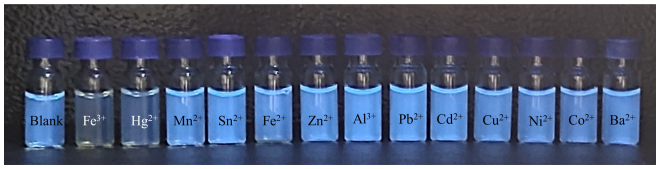

Figure 5. Photograph of sensing performance in the presence of various metal ions such as $FeCl_3$, $CuCl_2$, $CaCl_2$, $NiCl_2$, $CoCl_2$, $Zn(NO_3)_2$, $CdCl_2$, $PbSO_4$, $Al(NO_3)_3$, $HgCl_2$, $BaSO_4$, $MnCl_2$, and $SnCl_2$ observed under 365 nm.

7. Fluorescence Titration with Fe^{3+} and Hg^{2+} Addition

The fluorescence change was recorded with the incremental addition of Fe^{3+} metal ion upon excitation at 320 nm (please include Figure 7). From the fluorescence emission study, it was observed that as the Fe^{3+} and Hg^{2+} metal ion was added, there was a subsequent decrease in fluorescence, as shown in Figure 8. The CQD-TA-TRYP showed a response towards Fe^{3+} ion as it has more tendency to show interaction with -NH_2 and -OH containing groups. The quenching in fluorescence is observed mainly due to the photoinduced electron transfer phenomenon from excited state Tryp-CQD to half-filled orbital of Fe^{3+} metal ion. The strong fluorescence quenching is observed due to the transfer of electrons from CQD-TA-TRYP to empty 3d orbital of Fe^{3+} metal ion. In order to obtain deep insight into the binding affinity of CQD-TA-TRYP towards Fe^{3+} fluorescence, titration was performed. It was observed that as the Fe^{3+} was added to the CQD, fluorescence intensity decreases rapidly. The most plausible mechanism for fluorescence quenching is by transfer of electron or charge transfer process resulting in to non-radiative process leading to dynamic quenching. The fluorescence quenching occurs mainly due to the photoinduced electron transfer (PET) phenomenon.[25–30]

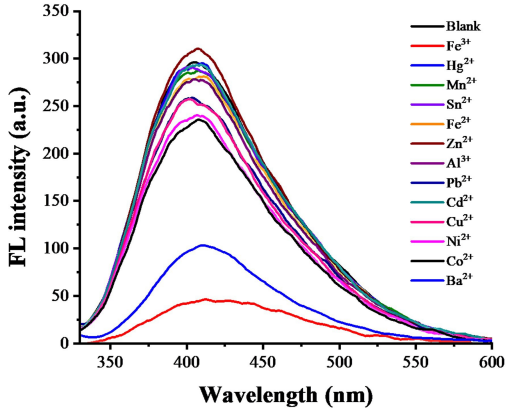

Figure 6. The emission spectra observed for the CQD-TA-TRYP with the addition of various metal ion such as Pb^{2+}, Fe^{3+}, Hg^{2+}, Al^{3+}, Co^{2+}, Cu^{2+}, Ni^{2+}, Zn^{2+}, Cd^{2+}, Mn^{2+}, Ba^{2+}, Fe^{2+}, and Sn^{3+} to the solutions containing CQD.

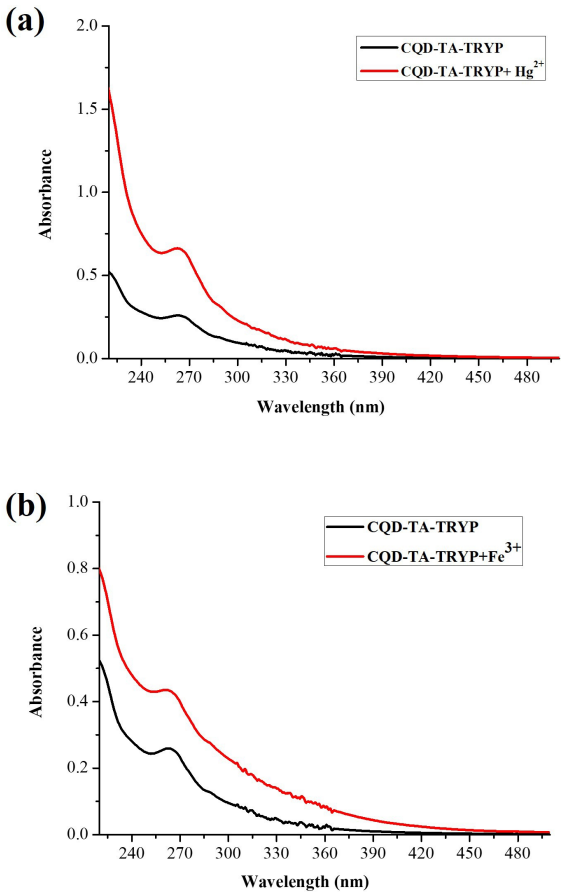

Figure 7. The absorption spectra observed for the CQD-TA-TRYP with the addition of metal ion (a) Hg^{2+} (b) Fe^{3+}.

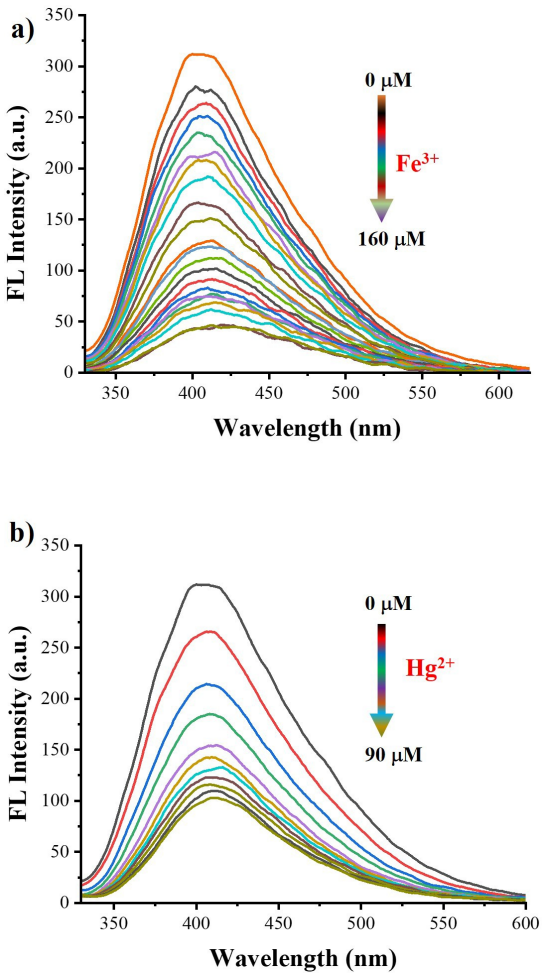

Figure 8. The Emission plot with the incremental addition of Fe^{3+} ion to CQD-TA-TRYP.

Similarly, the fluorescence study was performed for CQD-TA-TRYP as it was highly selective towards Hg^{2+} ions. The Tryp-CQD showed interaction with $-NH_2$ and $-OH$ groups present on the surface of the carbon dot. It is observed that initially, fluorescence intensity appeared at 400 nm and showed quenching with the addition of Hg^{2+} ion. However, to study its selectivity and binding capacity, fluorescent titration was performed with the incremental addition of Hg^{2+}.Figure 7.

8. Selectivity Study

The fluorescence response towards various cations was employed for the CQD-TA-TRYP to evaluate its selectivity. The selectivity study was performed in response to various cations such as Pb^{2+}, Fe^{3+}, Hg^{2+}, Al^{3+}, Co^{2+}, Cu^{2+}, Ni^{2+}, Zn^{2+}, Cd^{2+}, Mn^{2+}, Ba^{2+}, Fe^{2+}, and Sn^{3+}. It was observed that the CQD-TA-TRYP showed a significant response towards Fe^{3+} and Hg^{2+} metal ions in the presence of other competing cations. The response of fluorescence was recorded as exhibited in Figure S2, which shows clearly that the compound was highly selective towards Fe^{3+} and Hg^{2+} ions. Further, in order to gain a deeper insight into selectivity interference, a study was performed to explain its competitive nature. From the competitive study Figure 9. it was revealed that when different metal ions were added to the CQD-TA-TRYP solution, there was no quenching observed; however, to the same solution containing metal when Fe^{3+} and Hg^{2+} were added, there was complete quenching of fluorescence observed for the synthesized CQD. Thus, it is concluded that the addition of Fe^{3+} and Hg^{2+} showed quenching of fluorescence along with the competing interfering ion. The obtained results, revealed that there was no effect observed for metal ions other than Fe^{3+} and Hg^{2+} on the CQD. These results confirm that the CQD-TA-TRYP is well-suitable for sensing Fe^{3+} and Hg^{2+} metal ions.

9. Sensing Performance at Different PH

The effect of pH on the sensing performance of CQD-TA-TRYP was also examined and depicted in Figure 10. At pH 4, CQD-TA-TRYP exhibited low emission, which further decreased from 157.6 to 22 after the addition of Fe^{3+} ions. At pH 7, the emission intensity of the CQD-TA-TRYP significantly decreased from 285.7 to 56 after the addition of 160 μM of Fe^{3+} ions. Also, at pH 9.2,

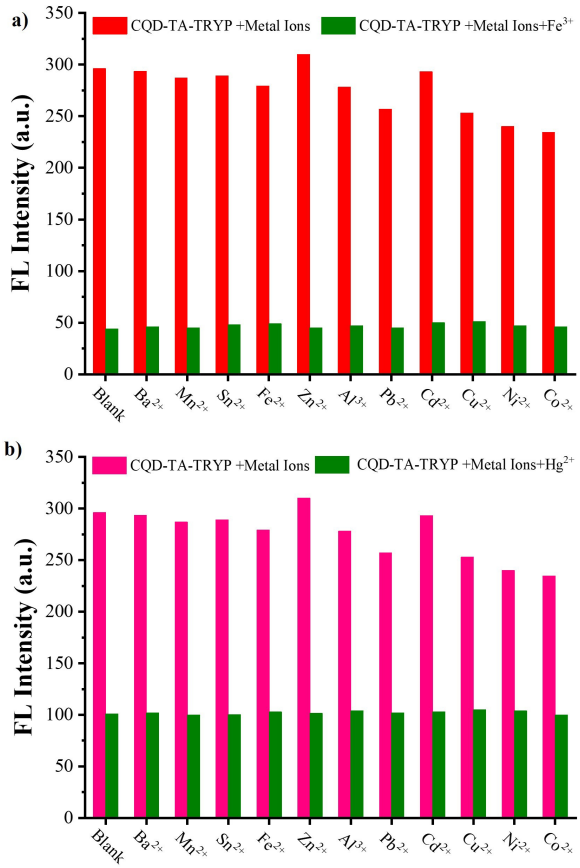

Figure 9. Fluorescence spectra of CQD-TA-TRYP exposed to various metal ions and the mixture of CQD-TA-TRYP and (a) Fe^{3+} and (b) Hg^{2+} ions in DW.

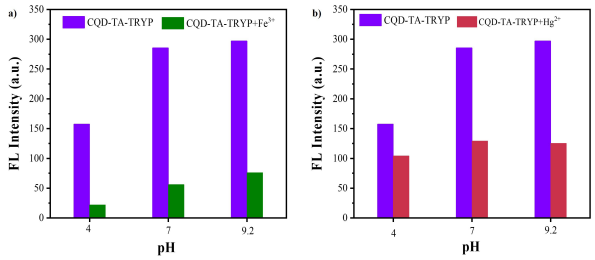

Figure 10. Sensing of (a) Fe^{3+} ions and (b) Hg^{2+} ions using **CQD-TA-TRYP** at different pH.

the emission intensity of CQD-TA-TRYP decreased from 297.2 to 76 after the addition of 160 μM of Fe^{3+} ions. Figure 10a.

The effect of pH was also examined in Hg^{2+} ions sensing, Figure 10b. At pH 4, the emission of CQD-TA-TRYP decreased slightly from 157.6 to 104 after the addition of Hg^{2+} ions. At pH 7, the emission intensity of the CQD-TA-TRYP decreased from 285.7 to 129.2 after the addition of 90 μM of Hg^{2+} ions. Also, at pH 9.2, the emission intensity of CQD-TA-TRYP decreased from 297.2 to 125.2 after the addition of 160 μM of Hg^{2+} ions.

10. Quenching Efficiency

The initial fluorescence intensity of CQD-TA-TRYP was found to show a significant decrease upon incremental addition of the Fe^{3+} ions and Hg^{2+} ions. The fluorescence quenching efficiency (η) of all the metal ions used was calculated using equation $[(I_0\text{-}I)/I_0] \times 100\,\%$, where I_0 and I are the fluorescence intensities before and after the addition of the various metal ions, such as Fe^{3+}, Hg^{2+}, Ba^{2+}, Mn^{2+}, Sn^{2+}, Fe^{2+}, Zn^{2+}, Al^{3+}, Pb^{2+}, Ni^{2+}, Co^{2+}, Cu^{2+}, and Cd^{2+} and results are shown in Figure 8. After the addition of 160 μM of Fe^{3+} ions and 90 μM of Hg^{2+} ions, the initial emission intensity of CQD-TA-TRYP was significantly decreased, and the quenching efficiency (η) was calculated to be about 88.05 % and 66 % for Fe^{3+} and Hg^{2+} ions respectively. Figure 11.

11. Stern Volmer Plot

The Stern Volmer constant (K_{SV}) was calculated by using fluorescence intensity (I_0/I) as a function of the concentration of [Q], which is calculated by the following equation: I_0/I=CQD-TA-TRYP + K_{sv}[Q]. The factors I_0 and I are the emission intensity before and after the addition of analyte Fe^{3+}, respectively, where K_{sv} is the quenching constant (M^{-1}) and [Q] is the molar concentration of Fe^{3+} analyte. From the Stern Volmer plot in Figure 9a, it can be noted that the Stern Volmer plot followed excellent linearity at a lower concentration of Fe^{3+} (90 μM); however, when the concentration is higher, the linearity deviated towards an upward direction. The Stern Volmer Plot with positive curvature results in intersystem crossing. It also results in a charge transfer complex in the ground and an excited state exhibiting both dynamic and static quenching. The obtained K_{sv} value for Fe^{3+} ion was observed to be $3\times10^4\ M^{-1}$. Thus, the results indicate that the Fe^{3+} metal ion shows a better quenching ability toward synthesized carbon dots studied in water. Figure 12a. Further, the Stern Volmer plot was evaluated for the CQD-TA-TRYP, which is highly selective towards Hg^{2+}. The K_{sv} for the Hg^{2+} ion was observed to be

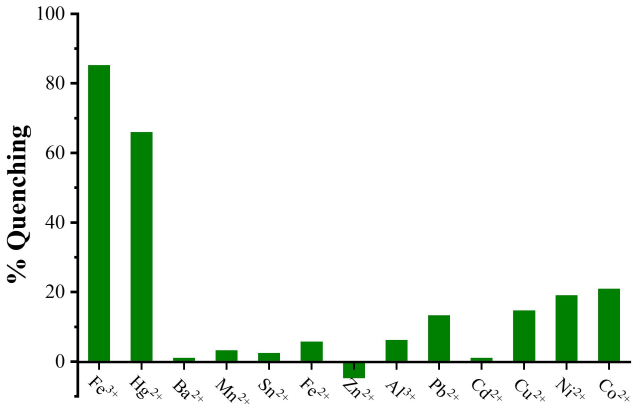

Figure 11. Fluorescence quenching of CQD-TA-TRYP by Fe^{3+}, Hg^{2+}, Ba^{2+}, Mn^{2+}, Sn^{2+}, Fe^{2+}, Zn^{2+}, Al^{3+}, Pb^{2+}, Ni^{2+}, Co^{2+}, Cu^{2+}, and Cd^{2+} metal ions.

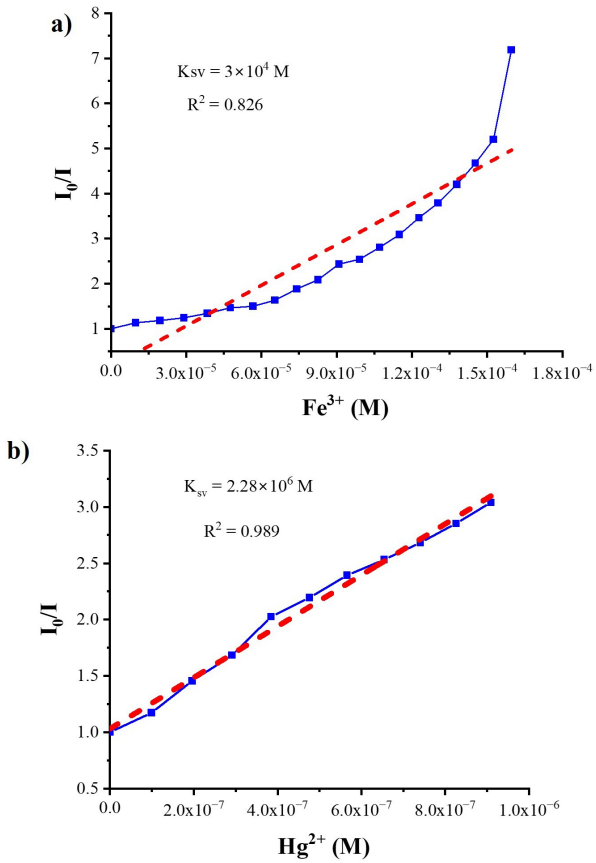

Figure 12. Stern–Volmer plot for **CQD-TA-TRYP** with (a) Fe^{3+} ions and (b) Hg^{2+} ions.

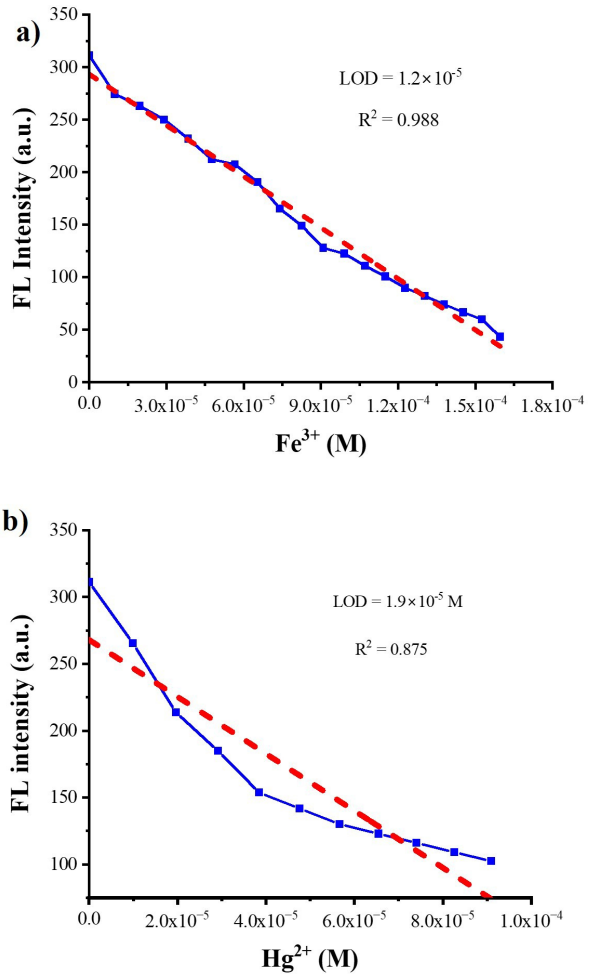

Figure 13. The linear fitting curve for determination of the limit of detection (LOD) (a) for Fe^{3+} ions and (b) for Hg^{2+} ions.

2.28×10^{6} M. This result also suggests that the synthesized CQD showed excellent linearity, as shown in Figure 12b.

12. Limit of Detection

The limit of detection was calculated by using formulae 3σ/m, where σ is the standard deviation of CQD-TA-TRYP. The detection limit was evaluated by performing fluorescence titration of synthesized CQD-TA-TRYP and Fe^{3+} metal ions with incremental addition of Fe^{3+} metal ion. The plot of the concentration of Fe^{3+} ion and fluorescent intensity was investigated. As the concentration of Fe^{3+} was increased from 0 to 160 μM, there was a decrease in fluorescence intensity linearly, as observed from the plot in Figure 13a. The difference in the emission intensity between the CQD-TA-TRYP and the concentration of Fe^{3+} before and after the addition was recorded.

The limit of detection for sensing of Fe^{3+} was found to be 1.2×10^{-5} M. By using a similar approach, the LOD was calculated for Hg^{2+}. The fluorescence intensity was recorded, and the plot of the concentration of Hg^{2+} with increasing emission intensity was plotted. There was a decrease in fluorescence intensity linearly, as observed from the plot in Figure 13b. The difference in the emission intensity between the CQD-TA-TRYP and the concentration of Fe^{3+} before and after the addition was recorded. Finally, the LOD detection for Hg^{2+} was observed to be 1.9×10^{-5} M.

13. Fluorescence Quenching Kinetics

Fluorescence quenching kinetics study was performed for the synthesized CQD-TA-TRYP carbon dot. In this study, the fluorescence quenching over the time course with addition of Hg^{2+} and Fe^{3+} metal ion (5 μM) was carried out. The fluorescence was recorded after every 5 minutes. The quenching of fluorescence observed over the period of 60 minutes as represented in Figure 14. The most plausible mechanism of fluorescence quenching of CQD by metal ion is related to the transfer of electron from photoexcitation of CQD to cation bound to its surface resulting in to non-radiative process. Thus, different quenching behaviours is observed with the addition of Fe^{3+} and Hg^{2+} metal ion.

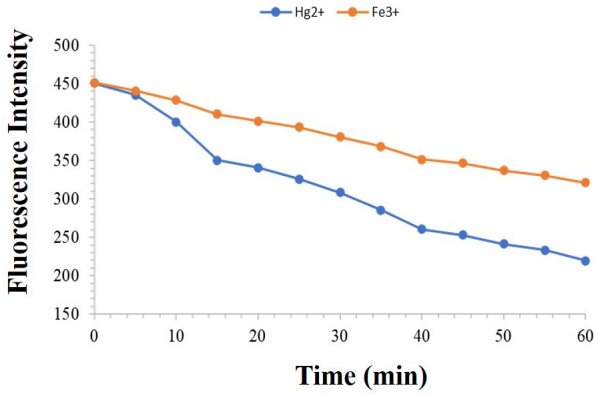

Figure 14. The kinetic study plot forFe^{3+} ions (red line) and for Hg^{2+} ions (blue line).

14. Water Analysis

The synthesized CQD-TA-TRYP was utilized for water analysis for detecting the trace ammount of Hg^{2+} and Fe^{3+} ion. In this application two water samples were selected form River Mandovi Goa and drinkingwater. Before analysis the water sample was preated. The river water sample was spiked with diffrent concentration as shown in Table 1 and Table 2 To this 25 μL of CQD-TA-TRYP was added and the solution was mixed. The emission was recorded after 5 minutes of spiking the analyte. The obtained percentage recovery for Hg^{2+} ion and Fe^{3+}in river water and tap water is as tabulated in Table 1 and Table 2 respectively.

15. Conclusions

In conclusion, CQD-TA-TRYP was synthesized by hydrothermal method using Tryptophan and tartaric acid, with high fluorescence quantum yield. The synthesized CQD was characterized successfully by FTIR, HR-TEM, UV-Vis, and fluorescence spectroscopy. It was observed that the CQD has a confined average size of 3.0 to 5.1 nm. with excellent dispersibility. It showed high stability under 365 nm UV light. In addition, the synthesized carbon dot has good solubility in water, and all analysis can be performed in aqueous medium, which is a greater advantage. After complete characterization, the compound was further utilized for sensing the application of various analytes. It was observed that the CQD can be utilized successfully for sensing Fe^{3+} and Hg^{2+} metal ions. The lowest detection limit of Fe^{3+} was found to be 1.2×10^{-5} M, while the LOD for Hg^{2+} ion was observed to be 1.9×10^{-5} M. The observed quenching efficiency was calculated to be 88.05% and 66% for Fe^{3+} and Hg^{2+} ions, respectively. Thus, from the obtained results, it can be concluded clearly that the molecule can be successfully utilized for sensing Fe^{3+} and Hg^{2+} metal ions. In addition, the synthesized carbon quantum dot can be used for water analysis application.

Table 1. Determination of Hg^{2+} ion in water sample.

Sr. No	Water Sample	Concentration (Hg^{2+} spiked)	Concentration (Hg^{2+} found)	% Recovery
1.	River water	6.25×10^{-5} M	6.20×10^{-5} M	99.2%
2.	Drinking water	3.75×10^{-5} M	3.85×10^{-5} M	102.6%

Table 2. Determination of Fe^{3+} ion in water sample.

Sr. No	Water Sample	Concentration (Fe^{3+} spiked)	Concentration (Fe^{3+} found)	% Recovery
1.	River water	6.25×10^{-5} M	6.15×10^{-5} M	98.4%
2.	Drinking water	8.7×10^{-5} M	8.7×10^{-5} M	100%

Experimental Section

Reagents and Materials

For the preparation of the carbon dots, various chemicals were purchased and used as is unless mentioned. Mainly, tartaric acid and tryptophan were purchased from TCI Chemicals Hyderabad, India, which was used without further purification. All the metal ions such as Fe^{3+}, Cu^{2+}, Ca^{2+}, Ni^{2+}, Co^{2+}, Cd^{2+}, Hg^{2+}, Mn^{2+}, and Cr^{3+}) were used as their chloride salt. Zn^{2+}, $Pb^{2+,}$ and Al^{3+} were used as their nitrate salt. Mg^{2+} and Ba^{2+} were used as their sulfate salts, respectively. The absorption and fluorescence emission properties were recorded on the Shimadzu UV-vis-1800 spectrophotometer and Agilent Cary Eclipse Spectro fluorophotometer, respectively. Quinine sulfate was used for calculating the quantum yield, which was purchased from Sigma Aldrich. All sample solutions were maintained at room temperature for spectrophotometric analysis, and all the analyses were carried out in pure distilled water.

Synthesis of CQD-TA-TRYP

The CQD-TA-TRYP were synthesized by conventional hydrothermal method using a Teflon-lined stainless steel hydrothermal vessel. Typically, CQDs were prepared using tartaric acid 500 mg and tryptophan 500 mg, dissolving in 10 ml of formamide. The reaction mixture was sonicated and placed in Teflon coated autoclave at 180 °C, which was kept for 12 h (Scheme 1). The obtained CQDs were cooled at room temperature, redispersed in ethyl acetate, and collected by centrifugation for 30 min. at 15000 rpm. The dark brown solution was further washed with acetonitrile to remove excess organic components. The obtained CQDs solution was characterized by FTIR analysis without any further purification (Scheme 2).

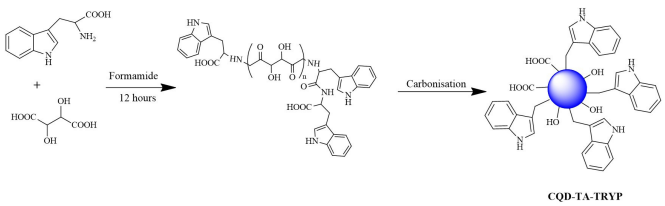

Scheme 1. Schematic representation for the synthesis of CQDs.

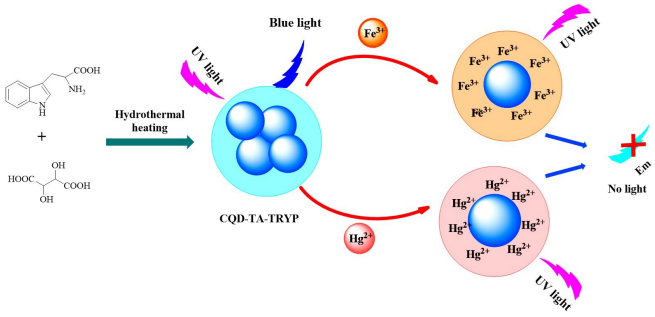

Scheme 2. The schematic representation for sensing of Fe^{3+} and Hg^{2+} ion.

Sensing Performance of Metal Ions

The sensing performance study toward various cations was performed at room temperature and by using distilled water. For this, the stock solution of CQD-TA-TRYP solution was prepared by dissolving 1 ml of liquid CQD-TA-TRYP in 10 ml distilled water. All metal ions stock solution was prepared in distilled water with appropriate concentration (~10^{-3} M). All the optical and fluorescence properties were executed in an aqueous medium using distilled water. The absorption and emission spectra were recorded by the addition of various cations in the CQD-TA-TRYP at room temperature.

Author Contributions

G.A.Z performed the synthesis and sensing application, and P.P.K and R.W.J. helped in the characterization and plotting of data and S.T.B. corrected the manuscript, and R.R.N and S.S. drafted the manuscript. S.V.B guided G.A.Z for the synthesis sequence analysis of data, characterization, and correction of the final manuscript. The Final manuscript is reviewed by all the Co-authors.

Acknowledgements

GAZ acknowledges DCTs Dhempe College of Arts and Science for the financial support. RWJ acknowledges joint UGC for NET Senior Research Fellowship. SVB acknowledges UGC-FRP for financial support and Professorship.

Conflict of Interests

The authors declare no conflict of interest.

Data Availability Statement

The data that support the findings of this study are available in the supplementary material of this article.

Keywords: Comparative chart · competitive plot · Stability study · Fluorescence · tryptophan

[1] J. Wei, J. Shen, X. Zhang, S. Guo, J. Pan, X. Hou, H. Zhang, L. Wang, B. Feng, *RSC Adv.* **2013**, *3*, 13119–13122.
[2] J. Y. Wan, Z. Yang, Z. G. Liu, H. X. Wang, *RSC Adv.* **2016**, *6*, 61292–61300.
[3] Y. Wang, A. Hu, *J. Mater. Chem. C* **2014**, *2*, 6921–6939.
[4] M. Esmaeili Koutamehr, M. Moradi, H. Tajik, R. Molaei, M. Khakbaz Heshmati, A. Alizadeh, *LWT-Ed.* **2023**, *184*, 114978.
[5] L. Zhu, D. Li, H. Lu, S. Zhang, H. Gao, *Int. J. Biol. Macromol.* **2022**, *194*, 254–263.
[6] D. Ozyurt, M. Al Kobaisi, R. K. Hocking, B. Fox, *Carbon Trends* **2023**, *12*, 100276, DOI 10.1016/j.cartre.2023.100276.
[7] D. Wang, L. Wang, X. Dong, Z. Shi, J. Jin, *Carbon* **2012**, *50*, 2147–2154.
[8] R. W. Jadhav, P. P. Khobrekar, S. T. Bugde, S. V. Bhosale, *Anal. Methods* **2022**, *14*, 3289–3298.
[9] S. Chahal, J. R. Macairan, N. Yousefi, N. Tufenkji, R. Naccache, *RSC Adv.* **2021**, *11*, 25354–25363.
[10] S. G. De Pedro, A. Salinas-Castillo, M. Ariza-Avidad, A. Lapresta-Fernández, C. Sánchez-González, C. S. Martínez-Cisneros, M. Puyol, L. F. Capitan-Vallvey, J. Alonso-Chamarro, *Nanoscale* **2014**, *6*, 6018–6024.
[11] J. Wang, Y. He, *Biomed. Appl. Toxicol. Carbon Nanomater.* **2016**, 429–486.
[12] A. S. Prayugo, Marpongahtun, S. Gea, A. Daulay, M. Harahap, J. Siow, R. Goei, A. I. Y. Tok, *Biosens. Bioelectron.* **2023**, *14*, 100363.
[13] J. Zuo, T. Jiang, X. Zhao, X. Xiong, S. Xiao, Z. Zhu, *J. Nanomater.* **2015**, *2015*, DOI 10.1155/2015/787862.
[14] Y. Wang, Y. Zhu, S. Yu, C. Jiang, *RSC Adv.* **2017**, *7*, 40973–40989.
[15] J. T. Clerc, *Fresenius Z. Anal. Chem.* **1980**, *300*, 8.
[16] T. V. De Medeiros, J. Manioudakis, F. Noun, J. R. Macairan, F. Victoria, R. Naccache, *J. Mater. Chem. C* **2019**, *7*, 7175–7195.
[17] S. Pandit, P. Behera, J. Sahoo, M. De, *ACS Appl. Bio Mater.* **2019**, *2*, 3393–3403.
[18] J. Yu, C. Xu, Z. Tian, Y. Lin, Z. Shi, *New J. Chem.* **2016**, *40*, 2083–2088.
[19] K. Fan, X. Wang, S. Yu, G. Han, D. Xu, L. Zhou, J. Song, *Polym. Chem.* **2019**, *10*, 5037–5043.
[20] C. Fan, L. Chen, R. Jiang, J. Ye, H. Li, Y. Shi, Y. Luo, G. Wang, J. Hou, X. Guo, *ACS Appl. Nano Mater.* **2021**, *4*, 4026–4036.
[21] M. R. Faraji, M. Mousazadeh, M. Nikkhah, A. Rezaei, S. Moradi, S. Hosseinkhani, *Int. J. Biol. Macromol.* **2024**, *260*, 129503.
[22] A. Rezaei, H. Zheng, S. Majidian, S. Samadi, A. Ramazani, *ACS Appl. Mater. Interfaces* **2023**, *47*, 54373–54385.
[23] A. Rezaei, M. A. Hamad, H. Adibi, H. Zheng, K. H. Qadir, *Mater Adv* **2024**, *5*, 1614–1625.
[24] Z. Yang, T. Xu, H. Li, M. She, J. Chen, Z. Wang, S. Zhang, J. Li, *Chem. Rev.* **2023**, *18*, 11047–11136.
[25] Y. Yang, T. Zou, Z. Wang, X. Xing, S. Peng, R. Zhao, X. Zhang, Y. Wang, *Nanomaterials* **2019**, *9*, 738.
[26] M. Maniyazagan, C. Rameshwaran, R. Mariadasse, J. Jeyakanthan, K. Premkumar, T. Stalin, *Sens. Actuators* **2017**, *242*,1227–1238.
[27] Z. Xiang, Y. Jiang, C. Cui, Y. Luo, Z. Peng, *Molecules* **2022**, *27*, 6749.
[28] F. Noun, E. A. Jury, R. Naccache, *Sensors* **2021**, *21*, 1391.
[29] A. Pal, S. Srivastava, P. Saini, S. Raina, P. P. Ingole, R. Gupta, S. Sapra, *J. Phys. Chem. C* **2015**, *119*, 22690–22699.
[30] E. Kalwarczyk, N. Ziebacz, T. Kalwarczyk, R. Holyst, M. Fialkowski, *Nanoscale* **2013**, *5*, 9908–9916.

Manuscript received: November 29, 2023